Measurement of incomplete fusion cross sections in ^{6,7}Li + ^{238}U reactions

A. Pal,[1,2,*] S. Santra,[1,2] D. Chattopadhyay,[1,2] A. Kundu,[1,2] A. Jhingan,[3] P. Sugathan,[3] B. K. Nayak,[1,2] A. Saxena,[1,2] and S. Kailas[1]

[1]*Nuclear Physics Division, Bhabha Atomic Research Centre, Mumbai 400085, India*
[2]*Homi Bhabha National Institute, Anushaktinagar, Mumbai 400094, India*
[3]*Inter University Accelerator Centre, Aruna Asaf Ali Marg, New Delhi 110067, India*

(Received 5 December 2018; published 27 February 2019)

Background: Incomplete fusion (ICF) in reactions involving weakly bound projectiles is understood to play an important role in enhancing the ratio of asymmetric to symmetric fission at $E \leqslant V_b$, widening the fission fragment folding angle distribution at $E \leqslant V_b$ and suppressing the complete fusion (CF) cross section at $E > V_b$. Experimental cross sections for individual ICF channels are necessary to obtain quantitative estimates of the above effects.

Purpose: Measurement of the cross sections for individual transfer-induced or ICF-fission channels in ^{6,7}Li + ^{238}U reactions to explain quantitatively the difference in the ratio of asymmetric to symmetric fission for total fission and CF fission.

Methods: Triple coincidence measurement of two fission fragments and one light charged projectilelike fragment (PLF) is carried out using two multiwire proportional counter (MWPC) detectors and an array of CSI(Tl) scintillation detectors at energies near the Coulomb barrier. By calculating the efficiency of the detectors by Monte Carlo simulation and fission probability by GEF code, the angle-integrated ICF cross sections corresponding to p, d, t, and α emission are obtained. Mass distributions for total fission are calculated by adding the distributions for CF fission and all ICF fissions with weight factors proportional to the measured cross sections.

Results: ICF cross sections corresponding to α emission are found to be the highest in both the reactions. The relative contribution of ICF to total fusion at the lowest measured energy is found to be $\approx$70% and it decreases with increasing projectile energy, consistent with the systematics of several reactions involving the same weakly bound projectiles. The simulated mass distributions for total fission are found to reproduce the experimental mass distributions.

Conclusions: Deuteron (triton) capture is observed to be the major ICF channel in the reaction involving ^{6}Li (^{7}Li) projectile. The ratio of the sum of ICF to total fusion cross section for the present systems are consistent with the systematics. The difference in the ratio of asymmetric to symmetric fission between total fission and CF fission is explained quantitatively.

DOI: 10.1103/PhysRevC.99.024620

I. INTRODUCTION

The study of fission reactions of nuclei populated in incomplete fusion or multinucleon transfer reaction is of great interest because of its wide applications in different areas. Indirect measurement of neutron-induced fission cross sections using the surrogate reaction technique [1–6] is one of them. Advantages of this technique are that one can populate a particular composite nuclide supposed to be formed by n-capture reaction without actually using the neutron beam and determine the cross sections for (n, f) reactions, and particularly, the same can be determined even for an unstable target and/or unstable projectile. The surrogate reaction technique can also be employed to study simultaneously the fission fragment mass distributions (FFMD) of several nuclei where fission is induced by multinucleon transfer [7–12] reactions. For example, Pal *et al.* has been able to measure simultaneously the FFMD of various neutron rich isotopes of Np and Pu, populated by the multinucleon transfer or incomplete fusion (ICF) channels in ^{6,7}Li + ^{238}U systems [9].

Besides the above applications, the ICF or transfer-induced fission also plays an important role in the dynamics of total fission. For example, the presence of ICF channels may modify (i) the ratio of asymmetric to symmetric fission mass distributions, (ii) the width of fission fragment folding angle distributions, and (iii) the anisotropy of fission fragment (FF) angular distributions. In the studies of Refs. [13,14] at sub-barrier energies, the presence of ICF or transfer-induced fission channels was attributed to be the reason for enhancing the peak to valley ratio ($P : V$) of the mass distribution and the width of folding angle distributions. Recently, the same has been confirmed by a direct measurement of fission fragment mass distributions for different ICF or transfer-induced fission channels in ^{6,7}Li + ^{238}U reactions [9]. It has also been confirmed that the folding angle distributions for individual

*asimpal@barc.gov.in

ICF fissions peak around the same angles where kinklike structures were observed in the folding angle distribution of total fission, thereby enhancing the width of the folding angle distributions of total fission at below barrier energies. In case of ICF fission, the excitation energy and angular momentum of the composite nucleus being different from the compound nucleus formed in CF, the fission fragment angular anisotropy is expected to be different. In a recent measurement of fission fragment angular distribution for ^{6}Li + ^{232}Th system [15], the angular anisotropy for a few ICF-fission channels was indeed found to be larger from the ones for CF fission. However, the overall angular anisotropy of total fusion (TF) fission including all recoil directions was found to be less than or equal to that of CF fission.

Another important feature of a reaction involving weakly bound stable projectiles (^{6,7}Li and ^{9}Be) is the suppression of complete fusion cross sections at energies above the Coulomb barrier [16–23]. Interestingly, it has been observed that the cross sections for incomplete fusion for some of these systems [24,25] are of similar order as that of the missing complete fusion cross sections.

The above examples lead to the fact that identification of different ICF channels and measurement of their cross sections are of utmost importance to understand many interesting features in reactions involving weakly bound projectiles. In literature, several methods have been employed to identify ICF channels, such as by measuring (i) recoil range distributions, (ii) fission fragment folding angle distributions, (iii) characteristic charge particle decay from composite nuclei, (iv) particle-γ coincidence, and (v) coincidence of fission fragments with light charged particles. The recoil range distribution method [26,27] is applied for measurements only at above barrier energies where the ranges of the recoils corresponding to CF and ICF are supposed to be different. However, practically it has been observed that the ranges have a good overlap leading to large uncertainties in the separation of CF and ICF contributions. Itkis *et al.* [13] have extracted the contributions of ICF channels from the multi-peak fit to the fission fragment folding angle distributions for ^{6}Li + ^{232}Th system. Different peaks of the folding angle distribution correspond to different ICF channels. Using the same method, Kailas *et al.* have estimated the transfer fission cross section for ^{11}B + ^{237}Np, ^{12}C + ^{236}U, and ^{16}O + ^{232}Th systems [28]. However, there are large uncertainties in the fit to such indistinct peaks that lead to large errors in the extracted cross sections. Using the third technique, Dasgupta *et al.* [24] have measured the ICF cross sections for the ^{6}Li + ^{209}Bi, ^{7}Li + ^{209}Bi, and ^{9}Be + ^{208}Pb reactions, at energies near and below the Coulomb barrier where the ICF channels have been identified by characteristic α decay from the composite system. It has been mentioned that some of these α emitting nuclei may have been originated from different ICF channels leading to uncertainties in individual ICF cross sections. Using the fourth technique, the ICF cross sections due to triton (t) or α capture have been measured using on-line and off-line γ counting for ^{7}Li + ^{124}Sn [25], ^{7}Li + ^{93}Nb [29], and ^{7}Li + ^{198}Pt [30] systems. In this technique, γ ray obtained in coincidence with the escaping particle has only been used to identify the composite system, but the cross sections have been determined from the inclusive γ counts. The fifth technique, i.e., light charged particle-fission coincidence technique has been used by Raabe *et al.* [31] to obtain ICF cross sections in ^{7}Li, ^{7,9}Be + ^{238}U reactions.

It may be pointed out that out of all the techniques mentioned above, the last technique, i.e., light charged-particle and fission-fragments coincidence technique is the most reliable, as the triple coincidence of two fission fragments and one light charged particle (the noncaptured projectile breakup fragment) confirms the occurrence of a specific ICF event. Whereas, the characteristic particle decay technique and the γ counting technique have the major disadvantage that the same composite system, which emits characteristic γ or particle, can be formed by different mechanisms (ICF or CF followed by particle evaporation).

In the present work, we have used the last technique, i.e., the light charged-particle and fission-fragment coincidence technique to measure the cross sections for individual ICF (with respect to p-, d-, t-, and α-gated) channels, for the ^{6,7}Li + ^{238}U reactions. These reactions have been chosen because we have already made several measurements on fission fragment mass and angular distributions for these two systems [9,14,32] and the present measurements will add further information towards the understanding of a complete fission reaction mechanism. It may be noted that p-, d-, t-, and α-gated ICF channels correspond to the captures of ^{5}He, α, ^{3}He, and d, respectively, in case of ^{6}Li projectile and captures of ^{6}He, ^{5}He, α, and t, respectively, in case of ^{7}Li projectile. An attempt has also been made to address the quantitative difference in $P:V$ ratio between total fusion fission and complete fusion fission as observed in Ref. [14], using the simulated mass distributions for inclusive fission by overlapping the distributions for complete fusion and all ICF fissions, taking into account proper weight factor proportional to the respective measured cross sections.

The paper is organized as follows. The experimental details are described in Sec. II. Details of the determination of experimental ICF cross sections for the present systems and a systematic study of the ratio of ICF to TF cross sections for several systems along with present systems have been described in Sec. III. A systematics of TF cross sections along with the coupled channel calculations have been described in Sec. IV. A description of the simulated mass distributions for total fission using the experimental mass distribution of CF fission and ICF fission is given in Sec. V. Finally, the results of the present study are summarized in Sec. VI.

II. EXPERIMENT AND DATA ANALYSIS

The experiment on ^{6,7}Li + ^{238}U reactions was carried out at 15-UD Pelletron facility in Inter University Accelerator Centre (IUAC), New Delhi. Three beam energies of 30, 34, and 40 MeV were used for ^{6}Li and two beam energies of 31.4 and 41.4 MeV were used for ^{7}Li. The ^{238}U target of thickness $\sim$100 μg/cm^2 was sandwiched between two layers of ^{12}C of thickness $\sim$15 μg/cm^2 each. Two position sensitive multiwire proportional counter (MWPC) detectors [33] were used to detect fission fragments. They were placed on two rotatable arms and kept on either side of the beam direction

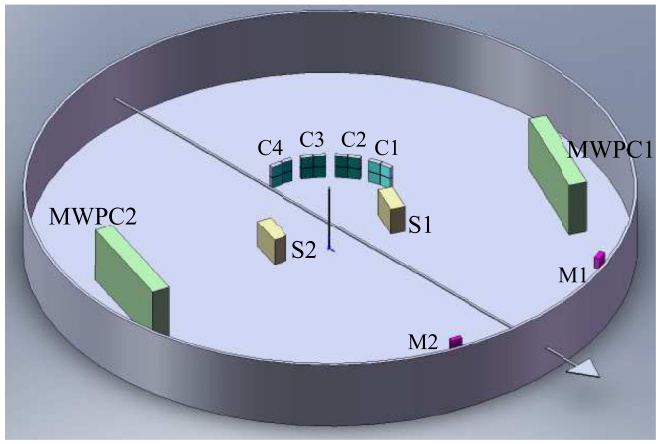

FIG. 1. Schematic diagram of the experimental setup inside the scattering chamber consisting of two MWPC detectors (MWPC1 and MWPC2) to detect fission fragments, two transmission-type START detectors (S1 and S2), four CsI(Tl) detectors (C1–C4) (4 × 4 crystals) to detect light charged particles, and two monitor detectors (M1 and M2) kept at ±10°.

making a folding angle of ≈172°–175°. A schematic diagram of the experimental setup has been shown in Fig. 1, same as in Ref. [9]. Each MWPC detector has an active area of 16 × 11 cm^2. The central distances of MWPC1 and MWPC2 from the target center were 39.5 cm and 33.5 cm, respectively. Each MWPC detector provides position information (horizontal and vertical) and a timing signal (STOP signal) for the time-of-flight (T1 and T2) measurements. The starts of the timing signals were taken from two transmission-type gas detectors of active area 3.7 × 3.7 cm^2 (S1 and S2) placed in front of the two MWPC detectors at a distance of 11 cm from the target center. Two monitor detectors (M1 and M2) were also used at ±10° to monitor the incident flux.

Four CsI(Tl) detectors having four crystals each [34] were used to detect projectilelike fragments (PLF) covering the angular range of 101°–168° for beam energies of 30, 31.4, and 34 MeV, and 71°–138° for beam energies of 40 and 41.4 MeV. The energy spectra of these detectors were calibrated using the known energies of α from a standard ^{229}Th source. Typical spectra corresponding to time correlation, coincidence TAC, and light charged-particle identification obtained from one of the CsI(Tl) detectors gated with MWPC detectors for ^{6}Li + ^{238}U reaction at a beam energy of 40 MeV are shown in Fig. 2. The correlation between the time-of-flight signals, T1 versus T2, obtained from two MWPC detectors has been shown in Fig. 2(a), which shows a clean spectrum of correlated fission events. Figure 2(b) shows the coincidence TAC spectrum between fission fragments and the PLFs. As mentioned in Ref. [9], the raw two-dimensional (2D) spectrum of PID versus energy measured in CsI detector has been gated with the above fission timing distributions (within red dashed contour) and the TAC spectrum (within the red dashed vertical lines). The resultant 2D spectrum thus obtained is shown in Fig. 2(c). It provides clear distinction between proton, deuteron, triton, and α bands.

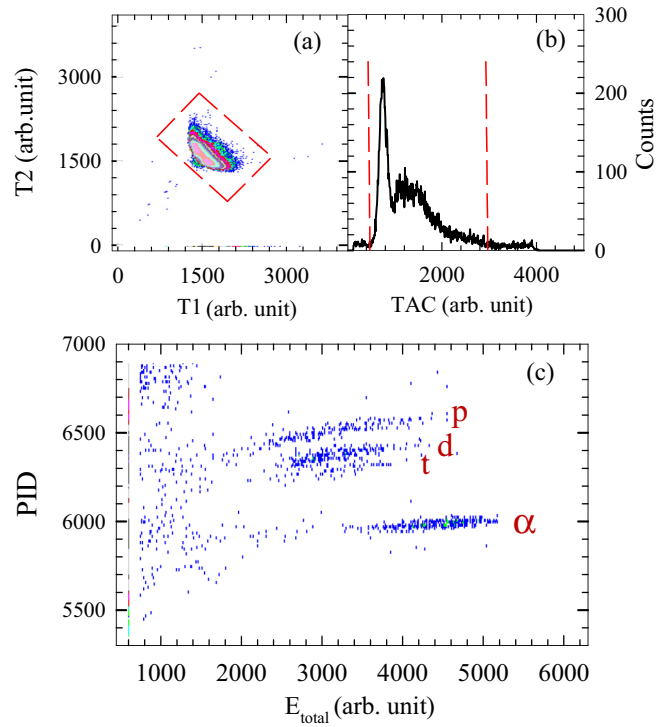

FIG. 2. Typical spectra involving 40 MeV ^{6}Li beam correspond to (a) 2D plot of the timings T1 versus T2 of the gas detectors MWPC1 and MWPC2, respectively, (b) 1D plot of the TAC between OR of MWPCs and OR of CsI(Tl) detectors, and (c) 2D plot of particle identification (PID) versus energy gated with the TAC and the banana gate on MWPC timings, shown in spectra (a).

III. INCOMPLETE FUSION CROSS SECTION

Incomplete fusion (ICF) is a process where one of the breakup fragments is captured by the target following the breakup of the projectile into two or more fragments. Sometimes, the same set of nucleons as that of the fragment may be directly transferred from the projectile to the target, making the stripping transfer reaction indistinguishable from the ICF process. If the target is in actinide region, after capturing the fragment, the composite system mostly undergoes fission. So, experimentally we can detect two fission fragments in coincidence with the escaping projectilelike fragment (the ejectile) without distinguishing the origin of the process, ICF or transfer. The ICF cross section, which includes transfer cross section as well, can be determined as follows. If $Y_{\rm coin}$ is the counts of the noncaptured projectilelike breakup fragments detected in coincidence with the two fission fragments, the differential ICF cross section can be written as

$$\frac{d\sigma}{d\Omega}(\theta) = \frac{Y_{\rm coin}}{Y_M}\frac{d\Omega_M}{d\Omega_{\rm CsI}}\frac{d\sigma_{\rm Ruth}}{d\Omega}\frac{1}{\epsilon}\frac{1}{P_f}, \tag{1}$$

where, Y_M is the number of counts at monitor detector, $d\Omega_M$, and $d\Omega_{\rm CsI}$ are the solid angles of monitor and CsI(Tl) scintillator detectors, respectively, $\frac{d\sigma_{\rm Ruth}}{d\Omega}$ is the Rutherford's differential scattering cross section at the scattering angle of the monitor (θ_M), ϵ is the fission-fission coincidence efficiency

and P_f is the fission probability followed by transfer or incomplete fusion. The efficiency ϵ mainly depends on two factors: (i) the FF coincidence efficiency between the two MWPC detectors (ϵ_1) and (ii) the geometric efficiency of the MWPC detectors (ϵ_2).

(i) *FF coincidence efficiency,* ϵ_1. Although the MWPC detectors have been placed in such a position that their central angles are at folding angles, but due to the finite width of the folding angle distribution, there is a chance that one of the two complementary fission fragments from a single fission event may miss the coincidence detection by the MWPC detectors. Hence, the interdetector coincidence efficiency has been determined using a Monte Carlo simulation assuming isotropic emissions of fission fragments in center of mass frame, though it is not a valid assumption since FF angular distribution is in general anisotropic. However, for the present systems, FF angular anisotropy being less (≈10–30%) [15,32,35], the above assumption is reasonable. Thus, using the Monte Carlo simulation, the interdetector coincidence efficiency (ϵ_1) has been obtained and found to be ≈70–80% for the present systems at all excitation energies.

(ii) *Geometric efficiency,* ϵ_2. Geometric efficiency of the MWPC detectors depend on the effective solid angle of the detectors. It can be calculated from the formula $\epsilon_2 = \frac{d\sigma_{\mathrm{MWPC1}}+d\sigma_{\mathrm{MWPC2}}}{4\pi}$.

Therefore, the product of ϵ_1 and ϵ_2 will be equal to the total coincidence efficiency (ϵ). Now P_f has been calculated using GEF code, version 2016/1.2 [36], where three main inputs are: fissioning nuclei, excitation energy, and RMS angular momentum (calculated assuming grazing collision in transfer reaction). P_f has been found to be ≈80–95% for all the fissioning systems at the measured excitation energies.

The FF-PLF coincidence counts will also depend on the position of the MWPC detectors, because of anisotropy of FF angular distribution. However, the anisotropy being small for the present systems at measured energy ranges, the ICF cross sections have been obtained by integrating the differential cross section over the all solid angles of PLF detectors.

$$\sigma_{\mathrm{ICF}} = \int \frac{d\sigma}{d\Omega}(\theta) d\Omega = 2\pi \int_0^{\pi} \frac{d\sigma}{d\Omega}(\theta) \sin\theta d\theta. \quad (2)$$

Following Eq. (1), the differential cross section as a function of θ_{cm} for α-, triton-, deuteron-, and proton-gated ICF reactions on $^{6}\mathrm{Li} + ^{238}\mathrm{U}$ system, have been obtained for 40 (red circle), 34 (blue square), and 30 MeV (pink star) projectile energies and shown in Figs. 3(a)–3(d), respectively.

Similarly, the differential cross section as a function of θ_{cm} for α-, triton-, deuteron-, and proton-gated ICF reactions on $^{7}\mathrm{Li} + ^{238}\mathrm{U}$ system, has been obtained for 41.4 (red circle) and 31.4 MeV (pink star) projectile energies and shown in Figs. 4(a)–4(d), respectively. In both the cases it is clearly observed that the differential cross section is the highest for α emission and lowest for proton emission at all the measured energies.

It may be noticed that the data presented in Figs. 3 and 4 are of limited angular range surrounding the peaks though they cover the majority of the cross sections. So, in order to get the angle-integrated cross section, a suitable fit with proper shape to the angular distribution data is necessary.

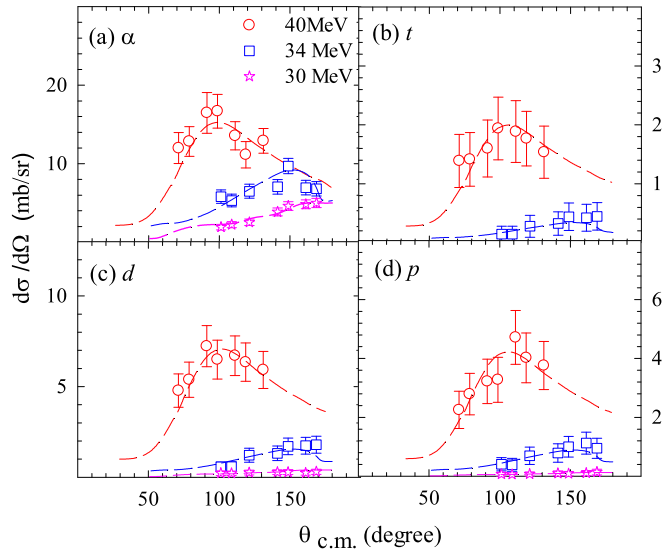

FIG. 3. The differential ICF cross sections at 40 MeV (red circle), 34 MeV (blue square), and 30 MeV (pink star) projectile energies corresponding to the ejectiles (a) α, (b) triton, (c) deuteron, and (d) proton in $^{6}\mathrm{Li} + ^{238}\mathrm{U}$ reaction. The fit to each of the data has been shown by dashed lines.

The shape of the angular distribution of the inclusive α cross section for reactions involving weakly bound projectiles is known to be similar to that of the transfer reaction, i.e., both of these reaction cross sections peak at the grazing angles [37]. In the present measurements the coincident PLF angular distributions at different energies indeed peak at the respective grazing angles. The shape of the angular distributions at a particular beam energy normalized to Coulomb barrier is

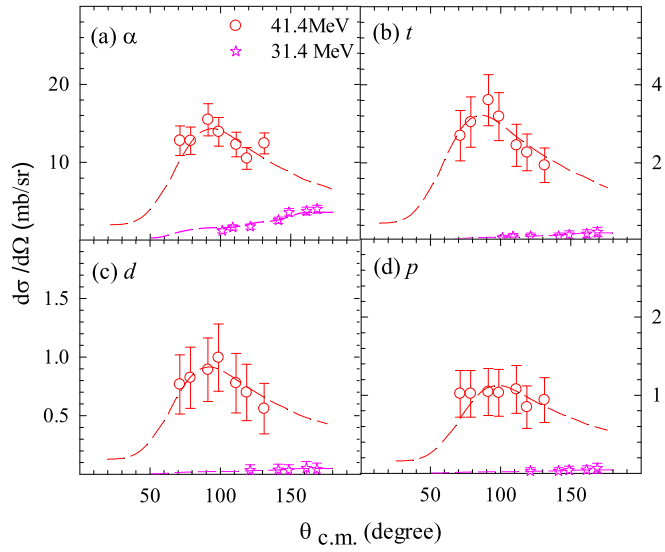

FIG. 4. The differential ICF cross sections at 41.4 MeV (red circle) and 31.4 MeV (pink star) projectile energies corresponding to the ejectiles (a) α, (b) triton, (c) deuteron, and (d) proton in $^{7}\mathrm{Li} + ^{238}\mathrm{U}$ reaction. The fit to each of the data has been shown by dashed line.

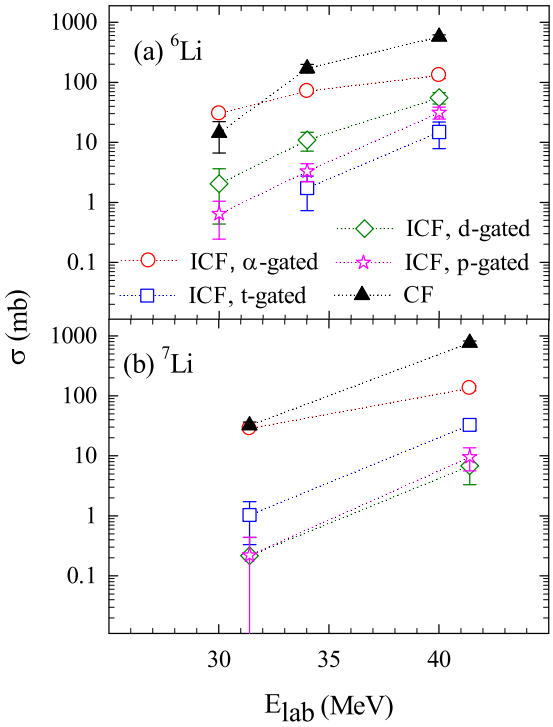

FIG. 5. The angle integrated ICF cross sections corresponding to the ejectile α (red circle), t (blue square), d (green diamond), and p (pink star) at different projectile energies for (a) ^{6}Li and (b) ^{7}Li. Black triangles represent CF cross sections estimated from the relation "$\sigma^{CF} = \sigma^{TF}$-$\Sigma_i \sigma_i^{ICF}$".

expected to be similar to that for a nearby system, e.g., ^{6}Li + ^{209}Bi [37]. Since the differential cross sections for inclusive α are available for a wide angular range at several near barrier beam energies, the shapes of these data at matching beam energy of E_{cm}/V_b has been used to fit the present data for each PLF angular distribution. The fits to the PLF angular distribution data corresponding to α-, t-, d-, and p-gated fissions are shown by dashed lines in Figs. 3 and 4.

Next, using Eq. (2), the angle integrated ICF cross sections corresponding to the outgoing noncaptured fragments such as α (red circle), t (blue square), d (green diamond), and p (pink star) have been obtained at different projectile energies as shown in Fig. 5(a) for ^{6}Li and 5(b) for ^{7}Li. It has been found that α emission is the most dominant ICF channel in both the reactions. The ICF cross sections have been observed to increase with increasing projectile energy, as expected. At higher ^{6}Li projectile energies the sequence of different ICF cross sections associated with different noncaptured fragments is observed to be $\sigma_\alpha > \sigma_d > \sigma_p > \sigma_t$, whereas for ^{7}Li, the sequence is $\sigma_\alpha > \sigma_t > \sigma_d > \sigma_p$. At lower projectile energies for ^{6}Li, $\sigma_p \sim \sigma_t$, whereas for ^{7}Li, $\sigma_p \sim \sigma_d$. The total ICF cross section at a particular beam energy has been obtained by summing all the individual ICF cross sections measured at that energy. The cross sections for CF have been estimated by subtracting total ICF cross sections from total fusion (TF) cross sections and the results are shown as black triangles in Fig. 5. The measured total ICF cross sections, existing TF cross sections from the literature [32,35] and the estimated CF cross sections have been given in Table I.

TABLE I. ICF, TF, and CF cross sections for ^{6,7}Li + ^{238}U systems.

Beam	Energy (MeV)	ICF x-section (mb)	TF x-section (mb)	CF x-section (mb)
	30	33 ± 3	47 ± 7	14 ± 7
^{6}Li	34	87 ± 7	258 ± 26	171 ± 27
	40	232 ± 22	807 ± 40	575 ± 46
	31.4	30 ± 2	62 ± 4	32 ± 5
^{7}Li	41.4	183 ± 15	950 ± 50	767 ± 52

A. Ratio of ICF to TF cross sections

To find the relative contribution of ICF to total fusion cross section, the ratio of cross section for ICF to TF, i.e., $\frac{\sigma_{ICF}}{\sigma_{TF}}$ has been determined from the measured data at different energies and shown in Fig. 6 as red filled (red hollow) circles for ^{6}Li (^{7}Li) + ^{238}U reaction. For a systematic study, the same quantity has been determined from the ICF and TF data available in the literature for several other systems involving weakly bound projectiles [24,25,30,31,38,39] and compared with the present data in Fig. 6. The relative contribution of ICF to TF for the present systems has been found to be the highest (≈70%) at the lowest measured energy and then it decreases with increasing energy, consistent with the trend for all the other systems obtained from the systematics. It is observed that the ICF to TF ratio for the present ^{6}Li + ^{238}U system is nearly equal to that of ^{6}Li + ^{209}Bi system [24] at near or below barrier energies. However, the ratio for ^{7}Li + ^{238}U

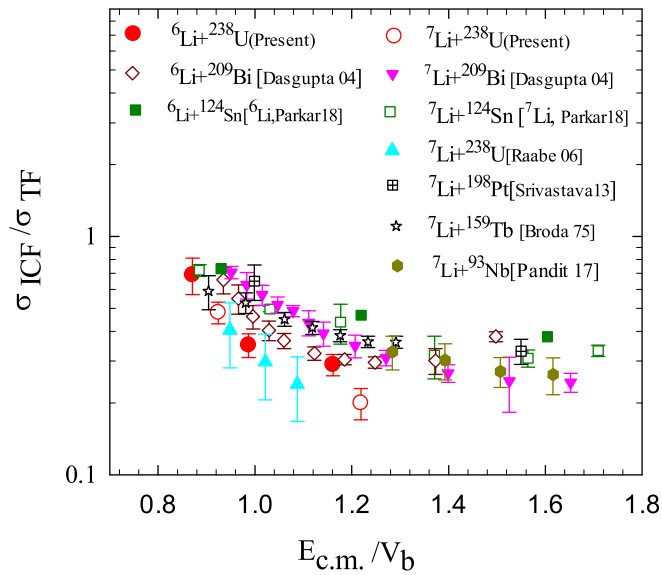

FIG. 6. The ratios of total ICF cross section to total fusion cross section for the present systems ^{6}Li + ^{238}U (red filled circles) and ^{7}Li + ^{238}U (red hollow circles) have been compared with the literature data for ^{7}Li + ^{124}Sn [25], ^{6}Li + ^{124}Sn [38], ^{6}Li + ^{209}Bi [24], and for ^{7}Li + ^{209}Bi [24], ^{7}Li + ^{238}U [31], ^{7}Li + ^{198}Pt [30], and ^{7}Li + ^{159}Tb [39].

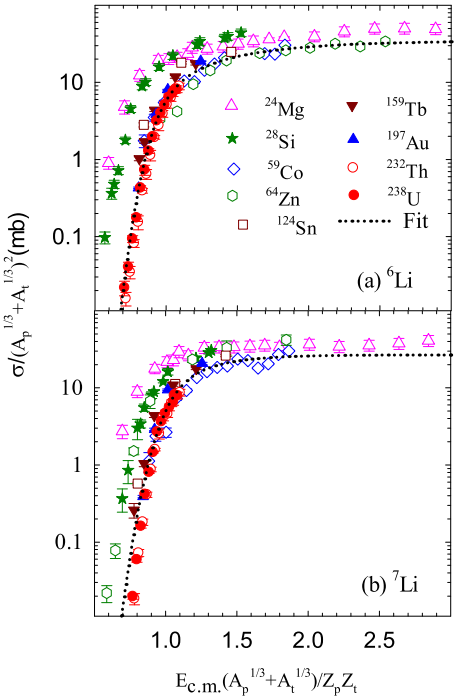

FIG. 7. A systematics of the total fusion (TF) cross sections for reactions involving several different targets such as ^{24}Mg [40], ^{28}Si [41,42], ^{59}Co [43], ^{64}Zn [44], ^{124}Sn [25,38], ^{159}Tb [25,38], ^{197}Au [45], and ^{232}Th [35] along with the present target ^{238}U (red filled circles) [35] with projectile (a) ^{6}Li and (b) ^{7}Li, respectively.

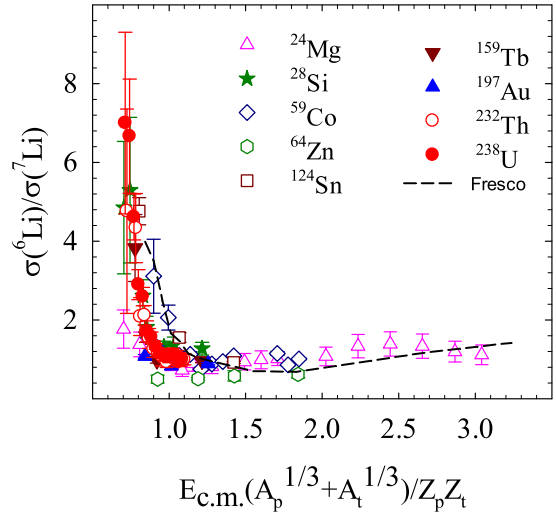

FIG. 8. A systematics of the ratio of total fusion (TF) cross sections for reactions involving ^{6}Li to ^{7}Li with several different targets like ^{24}Mg [40], ^{28}Si [41,42], ^{59}Co [43], ^{64}Zn [44], ^{124}Sn [25,38], ^{159}Tb [25,38], ^{197}Au [45]) and ^{232}Th [35] along with the present target ^{238}U (red filled circles) [35].

system obtained from the present measurement as well as from Ref. [31] is found to be slightly smaller than other systems available in the literature with ^{7}Li as a projectile. From the systematic study, it is interesting to note that the ratio of ICF to TF at above barrier energies is nearly equal to the complete fusion suppression factors for both the projectiles.

IV. SYSTEMATICS OF TF CROSS SECTIONS

To investigate any target dependence, the TF cross sections for the present systems have been compared with the ones available in the literature involving same projectile (either ^{6}Li or ^{7}Li), but different targets as a function of energy normalized to Coulomb barrier as shown in Fig. 7. It may be observed that the normalized TF cross sections for reactions involving heavier targets ($A \geqslant 124$) with both ^{6,7}Li projectiles follow a common trend [dotted lines in Figs. 7(a) and 7(b), respectively] with respect to the normalized beam energy. The reactions involving light targets, e.g., ^{24}Mg and ^{28}Si, are found to have larger TF cross sections compared to heavier targets, especially at sub-barrier energies. For reactions involving ^{59}Co with both ^{6,7}Li, the TF cross sections follow the same common trend (dotted lines) as of the heavier targets. However, for ^{64}Zn target, though the TF cross section involving ^{6}Li projectile follows the dotted line it does not follow for ^{7}Li projectile.

Further, to understand the role of projectile breakup threshold on ICF, the ratio of TF cross sections for reactions with ^{6}Li projectile to that with ^{7}Li projectile involving same target has been obtained as shown in Fig. 8. It may be observed that at above barrier energies the ratio is almost constant ($\approx$1) but as one moves down in energy below the barrier, the ratio increases sharply irrespective of the target mass. Qualitatively, one can understand this as follows. Due to low breakup threshold of ^{6}Li (compared to ^{7}Li), the breakup cross sections for reactions involving ^{6}Li are expected to be higher leading to higher ICF cross sections and hence higher TF cross sections than the reactions involving ^{7}Li. However, at near and sub-barrier energies the difference is expected to be much larger as a slight change in beam energy makes the excitation energy either above or below the breakup threshold depending upon the projectile. Thus, the cross section for breakup as well as fusion that vary exponentially with the excitation energy will make a huge difference in reactions involving two projectiles with different breakup thresholds at $E_{\text{beam}} \leqslant V_b$.

To understand the above energy dependence of the ratio of TF cross sections for ^{6}Li to ^{7}Li, coupled channels calculations using FRESCO (version 2.9) [46] have been performed. The continuum discretized coupled channels (CDCC) approach, similar to Refs. [47–49], has been considered to incorporate the effect of projectile breakup on fusion cross sections for $^{6}\text{Li} + ^{238}\text{U}$ and $^{7}\text{Li} + ^{238}\text{U}$ reactions, respectively. The short-ranged imaginary potentials considered for each of the outgoing channels absorb flux from the elastic and projectile breakup channels (assumed to be the major channels) correspond to total fusion cross section. For both $^{6,7}\text{Li} + ^{238}\text{U}$ reactions, all the resonant states and the nonresonant continuum above breakup threshold up to an excitation energy of about 8 MeV have been included. In case of $^{7}\text{Li} + ^{238}\text{U}$ reaction, the projectile bound excited state (0.48 MeV, $1/2^-$) has also been included. No target excitation was considered. The projectile ^{6}Li (^{7}Li) has been assumed to have a two-body cluster structure of $\alpha + d$ ($\alpha + t$) with the breakup threshold (E_{th}) of 1.48 (2.47) MeV. The continuum of $\alpha + d$ ($\alpha + t$) cluster of

^{6}Li (^{7}Li) at $E > E_{\rm th}$, has been discretized with respect to the α-d (α-t) relative momentum of $\hbar k$ into several momentum bins, in steps of $\Delta k = 0.2$ fm^{-1}, up to $k = 0.8$ fm^{-1} [50]. Each bin has been treated as an excited state of $\alpha + d$ ($\alpha + t$) cluster with excitation energy equal to the mean excitation. An average wave function, assumed to be independent of energy within the bin width, has been normalized to unity. The spin of the excited state has been obtained as the vector sum of the α-d (α-t) relative angular momentum L and the spin of the deuteron (triton) S. All possible states with $L = 0, 1, 2$ ($L = 0, 1, 2, 3$) have been included. The binning of the continuum of ^{6}Li (^{7}Li) with $L = 2$ ($L = 3$) has been suitably modified to include the resonance states with average excitation energies matching with the resonance energies.

The CDCC calculations were performed using cluster-folded (CF) interactions, where Sao Paolo potentials [51] were used as the real parts of the fragment target ($\alpha + ^{238}$U and $d + ^{238}$U or $t + ^{238}$U) potentials. The imaginary potentials for the above three interactions were taken to be short ranged and Woods-Saxon squared form with $W = 10$ MeV, $r_w = 0.8$ fm, and $a_w = 0.2$ fm. The $\alpha + d$ and $\alpha + t$ binding potentials of Ref. [52], suitably modified for resonances that generate proper phase shifts, have been used.

The total absorption cross sections (considered as TF cross sections) obtained from the above calculations have been used to calculate the ratio of TF cross sections for ^{6}Li + ^{238}U to ^{7}Li + ^{238}U reactions and shown as a dashed line in Fig. 8. The theoretical results have a reasonable agreement with the trend of the experimental data, which is almost independent of target mass. It implies that the difference in TF or ICF cross sections for ^{6}Li and ^{7}Li is a direct consequence of the effect of projectile breakup threshold for all the systems studied here.

V. UNDERSTANDING MASS DISTRIBUTION OF TF FISSION

As stated in Sec. I, a difference in peak to valley ratio ($P : V$) of mass distributions between TF fission and CF fission has been observed in ^{6,7}Li + ^{238}U reactions [14] and ICF fission was assumed to be the reason for this discrepancy. In our recent work [9], the mass distributions of the nuclei populated in those ICF channels have been measured for the same reactions and the $P : V$ ratio of all the ICF channels (α-, t-, d-, and p-gated fissions) have been already obtained. In the present study, it has been possible to determine the cross sections for individual ICF and CF channels (see Fig. 5 and Table I). So, one can now explain the experimental mass distribution for TF fission as a combination of the mass distribution of CF and ICF fissions with appropriate weight factors proportional to their respective cross sections.

A typical case of mass distribution measured in ^{6}Li + ^{238}U reaction at the beam energy of 30 MeV, where the difference between CF and TF fission is maximum, has been considered for the above purpose. An overlap of the mass distributions of all ICF channels with the CF channel with proper weight factor proportional to the measured cross sections has been obtained. The percentage contribution of CF and different ICF fissions to total fission is given in Table II. In Fig. 9, the fitted curves of the experimental mass distributions for CF, α-gated, t-gated, d-gated, and p-gated fission events obtained from Ref. [9] have been shown by black dotted, red short-dashed, pink long-dashed, blue dash-dotted, and green dash-dot-dotted lines. The black hollow circles and red filled circles represent the experimental mass distributions for CF and TF fissions, respectively. Using the above fitted mass distributions of CF and individual ICF channels an overlap of all the mass distributions has been obtained employing the following relation:

$$Y_{\rm TF}(m) = \frac{\sigma_{\rm CF} Y_{\rm CF}(m) + \sum_i \sigma_{i-\rm gated} Y_{i-\rm gated}(m)}{\sigma_{\rm TF}} \quad (i = \alpha, t, d, p). \tag{3}$$

The overlapping mass-distribution thus obtained for total fission has been shown as the red solid line in Fig. 9. It is clearly observed that $P : V$ ratio of the overlapping mass-distribution is larger than the one for CF fission. Similar exercise has been carried out at remaining energies for ^{6}Li + ^{238}U as well as ^{7}Li + ^{238}U systems and the results for the $P : V$ ratios obtained from the simulated mass distributions for the TF fission have been compared with the ones obtained from

TABLE II. Percentage contributions of CF, α-gated, t-gated, d-gated, and p-gated fission in ^{6,7}Li + ^{238}U reactions.

Beam	Energy (MeV)	CF (%)	α-gated (%)	t-gated (%)	d-gated (%)	p-gated (%)
	30	31 ± 17	64 ± 11	–	4.3 ± 3.4	1.4 ± 0.8
^{6}Li	34	66 ± 12	28 ± 4	0.7 ± 0.4	4.2 ± 1.5	1.3 ± 0.4
	40	71 ± 7	16 ± 2	1.8 ± 0.9	6.9 ± 1.5	3.9 ± 0.9
	31.4	52 ± 8	46 ± 4	1.7 ± 1.1	0.4 ± 0.3	0.3 ± 0.3
^{7}Li	41.4	81 ± 7	14 ± 2	3.5 ± 0.5	0.7 ± 0.4	1.0 ± 0.4

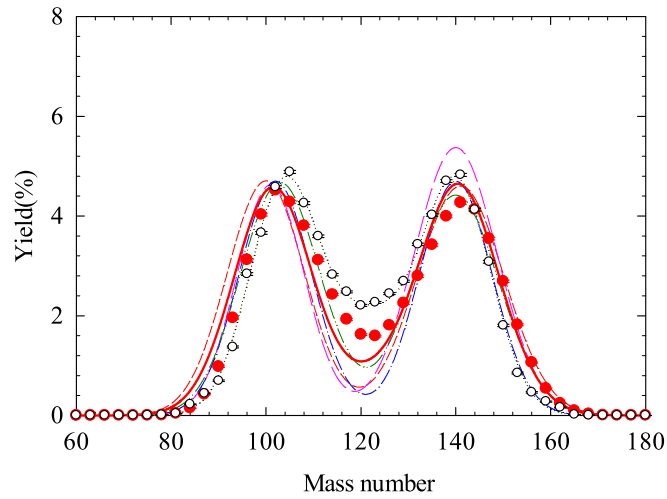

FIG. 9. Mass distributions for CF fission and α-, t-, d-, and p-gated fission have been shown by black dotted, red short-dashed, pink long-dashed, blue dash-dotted, and green dash-dot-dotted lines, respectively, for 30 MeV ^{6}Li + ^{238}U system. The overlapping mass distributions obtained from Eq. (3) have been shown by solid red line.

TABLE III. Calculated and experimental P : V ratios of TF fission mass distributions for ^{6,7}Li + ^{238}U systems.

Beam	Energy (MeV)	$(P/V)_{\text{calculated}}$	$(P/V)_{\text{experimental}}$
	30	3.9 ± 2.0	2.80 ± 0.10
^{6}Li	34	2.3 ± 0.9	2.00 ± 0.05
	40	1.9 ± 0.5	1.56 ± 0.01
	31.4	3.2 ± 1.8	2.39 ± 0.10
^{7}Li	41.4	1.66 ± 0.3	1.56 ± 0.01

the measurements [9,14] in Table III. The calculated $P : V$ ratios of the simulated mass distributions for TF fission are found to be consistent with the experimental values within experimental uncertainty.

VI. SUMMARY

The cross sections for individual transfer-induced fission or incomplete-fusion fission channels in ^{6,7}Li + ^{238}U reactions have been measured using the fission-fragments and light- charged-particle coincidence technique. In this triple coincidence measurement, the two fission fragments were detected using large area MWPC detectors and the light charge particles were detected using CsI detectors. The coincidence efficiency between two MWPC detectors, required for calculating cross sections, has been determined using a Monte Carlo simulation.

The cross sections for incomplete fusion have also been obtained at different energies by multiplying the above ICF-fission cross sections by the respective excitation energy dependent fission probabilities calculated using GEF code (version 2016.VI.1.2) [36].

It may be noted that the p-, d-, t-, and α-gated ICF channels correspond to the captures of ^{5}He, α, ^{3}He, and d, respectively, in case of ^{6}Li projectile and captures of ^{6}He, ^{5}He, α, and t, respectively, in case of ^{7}Li projectile. The cross sections for ICF followed by d capture and t capture for ^{6}Li and ^{7}Li projectile, respectively, have been found to be the most significant channels at all the measured energies. Total ICF cross sections for a projectile energy have been obtained by adding individual ICF channels measured at that beam energy. The ratio of total ICF cross section to total (CF+ICF) fusion cross section have been obtained and compared with the literature data. Interestingly, the ratio of ICF to TF at above barrier energies for ^{6}Li (^{7}Li) + ^{238}U reaction was found to be ≈30% (20%), which is of same order as the complete fusion suppression factor commonly observed in reactions involving weakly bound projectile ^{6}Li (^{7}Li).

A systematic study of the TF cross sections for ^{6}Li and ^{7}Li projectiles involving same target has been made and compared with the present systems and coupled channels calculations. The ratio of TF cross sections for ^{6}Li to that of ^{7}Li is found to increase with the decrease in energy (irrespective of the target) at sub-barrier energies manifesting the effect of projectile breakup threshold.

The overlapping distributions of CF-fission and all the ICF-fission channels with appropriate weight factors proportional to the measured CF and ICF cross sections were found to reasonably reproduce the experimental mass distributions for TF fission and thus quantitatively explain the difference in the peak to valley ratios between TF and CF fission for the present systems.

ACKNOWLEDGMENTS

We would like to thank the Pelletron crew for the smooth operation of the accelerator during the experiments.

[1] A. Pal, S. Santra, B. K. Nayak, K. Mahata, V. V. Desai, D. Chattopadhyay, and R. Tripathi, Phys. Rev. C **91**, 054618 (2015).
[2] B. K. Nayak, A. Saxena, D. C. Biswas, E. T. Mirgule, B. V. John, S. Santra, R. P. Vind, R. K. Choudhury, and S. Ganesan, Phys. Rev. C **78**, 061602(R) (2008).
[3] V. V. Desai, B. K. Nayak, A. Saxena, D. C. Biswas, E. T. Mirgule, B. John, S. Santra, Y. K. Gupta, L. S. Danu, G. K. Prajapati *et al.*, Phys. Rev. C **87**, 034604 (2013).
[4] V. V. Desai, B. K. Nayak, A. Saxena, E. T. Mirgule, and S. V. Suryanarayana, Phys. Rev. C **88**, 014613 (2013).
[5] H. C. Britt and J. D. Cramer, Phys. Rev. C **2**, 1758 (1970).
[6] J. E. Escher, J. T. Burke, F. S. Dietrich, N. D. Scielzo, I. J. Thompson, and W. Younes, Rev. Mod. Phys. **84**, 353 (2012).
[7] R. Leguillon, K. Nishio, K. Hirose, H. Maki, I. Nishinaka, R. Orlandia, K. Tsukada, J. Smallcombe, S. Chiba, Y. Aritomod *et al.*, Phys. Lett. B **761**, 125 (2016).
[8] K. Hirose, K. Nishio, S. Tanaka, R. Leguillon, H. Makii, I. Nishinaka, R. Orlandi, K. Tsukada, J. Smallcombe, M. J. Vermeulen *et al.*, Phys. Rev. Lett. **119**, 222501 (2017).
[9] A. Pal, S. Santra, D. Chattopadhyay, A. Kundu, A. Jhingan, P. Sugathan, N. Saneesh, M. Kumar, N. L. Singh, A. Yadav *et al.*, Phys. Rev. C **98**, 031601(R) (2018).
[10] E. Konecny, H. Specht, and J. Weber, Phys. Lett. B **45**, 329 (1973).
[11] K. Nishio, H. Ikezoe, Y. Nagame, S. Mitsuoka, I. Nishinaka, L. Duan, K. Satou, S. Goto, M. Asai, H. Haba *et al.*, Phys. Rev. C **67**, 014604 (2003).
[12] E. K. Hulet, R. W. Lougheed, J. H. Landrum, J. F. Wild, D. C. Hoffman, J. Weber, and J. B. Wilhelmy, Phys. Rev. C **21**, 966 (1980).
[13] I. Itkis, A. Bogacheva, A. Chizhov, D. Gorodisskiy, M. Itkis, G. Knyazheva, N. Kondratiev, E. Kozulin, L. Krupa, S. Mulgin *et al.*, Phys. Lett. B **640**, 23 (2006).
[14] S. Santra, A. Pal, P. K. Rath, B. K. Nayak, N. L. Singh, D. Chattopadhyay, B. R. Behera, V. Singh, A. Jhingan, P. Sugathan *et al.*, Phys. Rev. C **90**, 064620 (2014).
[15] A. Pal, S. Santra, D. Chattopadhyay, A. Kundu, K. Ramachandran, R. Tripathi, B. J. Roy, T. N. Nag, Y. Sawant, D. Sarkar *et al.*, Phys. Rev. C **96**, 024603 (2017).

[16] L. F. Canto, P. R. S. Gomes, R. Donangelo, J. Lubian, and M. S. Hussein, Phys. Rep. **596**, 1 (2015).

[17] P. K. Rath, S. Santra, N. L. Singh, R. Tripathi, V. V. Parkar, B. K. Nayak, K. Mahata, R. Palit, S. Kumar, S. Mukherjee *et al.*, Phys. Rev. C **79**, 051601(R) (2009).

[18] C. S. Palshetkar, S. Santra, A. Chatterjee, K. Ramachandran, S. Thakur, S. K. Pandit, K. Mahata, A. Shrivastava, V. V. Parkar, and V. Nanal, Phys. Rev. C **82**, 044608 (2010).

[19] V. V. Parkar, R. Palit, S. K. Sharma, B. S. Naidu, S. Santra, P. K. Joshi, P. K. Rath, K. Mahata, K. Ramachandran, T. Trivedi *et al.*, Phys. Rev. C **82**, 054601 (2010).

[20] M. K. Pradhan, A. Mukherjee, P. Basu, A. Goswami, R. Kshetri, R. Palit, V. V. Parkar, M. Ray, S. Roy, P. R. Chowdhury *et al.*, Phys. Rev. C **83**, 064606 (2011).

[21] P. K. Rath, S. Santra, N. L. Singh, K. Mahata, R. Palit, B. K. Nayak, K. Ramachandran, V. V. Parkar, R. Tripathi, and S. K. Pandit, Nucl. Phys. A **874**, 14 (2012).

[22] P. K. Rath, S. Santra, N. L. Singh, B. K. Nayak, K. Mahata, R. Palit, K. Ramachandran, S. K. Pandit, A. Parihari, A. Pal *et al.*, Phys. Rev. C **88**, 044617 (2013).

[23] A. Kundu, S. Santra, A. Pal, D. Chattopadhyay, B. K. Nayak, A. Saxena, and S. Kailas, Phys. Rev. C **94**, 014603 (2016).

[24] M. Dasgupta, P. R. S. Gomes, D. J. Hinde, S. B. Moraes, R. M. Anjos, A. C. Berriman, R. D. Butt, N. Carlin, J. Lubian, C. R. Morton *et al.*, Phys. Rev. C **70**, 024606 (2004).

[25] V. V. Parkar, S. K. Sharma, R. Palit, S. Upadhyaya, A. Shrivastava, S. K. Pandit, K. Mahata, V. Jha, S. Santra, K. Ramachandran *et al.*, Phys. Rev. C **97**, 014607 (2018).

[26] J. M. Alexander and G. N. Simonoee, Phys. Rev. **162**, 952 (1967).

[27] R. Bimbot, D. Gardes, and M. Rivet, Nucl. Phys. A **189**, 193 (1972).

[28] S. Kailas, D. M. Nadkarni, A. Chatterjee, A. Saxena, S. S. Kapoor, D. Chattopadhyay, R. Vandenbosch, J. P. Lestone, J. F. Liang, D. J. Prindle *et al.*, Phys. Rev. C **59**, 2580 (1999).

[29] S. K. Pandit, A. Shrivastava, K. Mahata, V. V. Parkar, R. Palit, N. Keeley, P. C. Rout, A. Kumar, K. Ramachandran, S. Bhattacharyya *et al.*, Phys. Rev. C **96**, 044616 (2017).

[30] A. Shrivastava, A. Navin, A. Diaz-Torres, V. Nanal, K. Ramachandran, M. Rejmund, S. Bhattacharyya, A. Chatterjee, S. Kailas, A. Lemasson *et al.*, Phys. Lett. B **718**, 931 (2013).

[31] R. Raabe, C. Angulo, J. L. Charvet, C. Jouanne, L. Nalpas, P. Figuera, D. Pierroutsakou, M. Romoli, and J. L. Sida, Phys. Rev. C **74**, 044606 (2006).

[32] A. Parihari, S. Santra, A. Pal, N. L. Singh, K. Mahata, B. K. Nayak, R. Tripathi, K. Ramachandran, P. K. Rath, R. Chakrabarti *et al.*, Phys. Rev. C **90**, 014603 (2014).

[33] A. Jhingan, P. Sugathan, K. S. Golda, R. P. Singh, T. Varughese, H. Singh, B. R. Behera, and S. K. Mandal, Rev. Sci. Instrum. **80**, 123502 (2009).

[34] A. Jhingan, P. Sugathan, G. Kaur, K. Kapoor, N. Saneesh, T. Banerjee, H. Singh, A. Kumar, B. Behera, and B. Nayak, Nucl. Instrum. Methods Phys. Res. A **786**, 51 (2015).

[35] H. Freiesleben, G. T. Rizzo, and Z. R. Huizenga, Phys. Rev. C **12**, 42 (1975).

[36] B. Jurado and K. H. Schmidt, Computer code GEF, version 1.2 (2016), http://www.khs-erzhausen.de/GEF-2016-1-2.html

[37] S. Santra, S. Kailas, V. V. Parkar, K. Ramachandran, V. Jha, A. Chatterjee, P. K. Rath, and A. Parihari, Phys. Rev. C **85**, 014612 (2012).

[38] V. V. Parkar, S. K. Pandit, A. Shrivastava, R. Palit, K. Mahata, V. Jha, K. Ramachandran, S. Gupta, S. Santra, S. K. Sharma *et al.*, Phys. Rev. C **98**, 014601 (2018).

[39] R. Broda, M. Ishihara, B. Herskind, H. Oeschler, and S. Ogaza, Nucl. Phys. A **248**, 356 (1975).

[40] M. Ray, A. Mukherjee, M. K. Pradhan, R. Kshetri, M. S. Sarkar, R. Palit, I. Majumdar, P. K. Joshi, H. C. Jain, and B. Dasmahapatra, Phys. Rev. C **78**, 064617 (2008).

[41] M. Sinha, H. Majumdar, P. Basu, S. Roy, R. Bhattacharya, M. Biswas, M. Pradhan, R. Palit, I. Mazumdar, and S. Kailas, Eur. Phys. J. A **44**, 403 (2010).

[42] A. Pakou, K. Rusek, N. Alamanos, X. Aslanoglou, M. Kokkoris, A. Lagoyannis, T. J. Mertzimekis, A. Musumarra, N. G. Nicolis, D. Pierroutsakou *et al.*, Eur. Phys. J. A **39**, 187 (2009).

[43] C. Beck, F. A. Souza, N. Rowley, S. J. Sanders, N. Aissaoui, E. E. Alonso, P. Bednarczyk, N. Carlin, S. Courtin, A. Diaz-Torres *et al.*, Phys. Rev. C **67**, 054602 (2003).

[44] A. D. Pietro, P. Figuera, E. Strano, M. Fisichella, O. Goryunov, M. Lattuada, C. Maiolino, C. Marchetta, M. Milin, A. Musumarra, V. Ostashko, M. G. Pellegriti, V. Privitera, G. Randisi, L. Romano, D. Santonocito, V. Scuderi, D. Torresi, and M. Zadro, Phys. Rev. C **87**, 064614 (2013).

[45] C. S. Palshetkar, S. Thakur, V. Nanal, A. Shrivastava, N. Dokania, V. Singh, V. V. Parkar, P. C. Rout, R. Palit, R. G. Pillay *et al.*, Phys. Rev. C **89**, 024607 (2014).

[46] I. J. Thompson, Comput. Phys. Rep. **7**, 167 (1988).

[47] S. Santra, V. V. Parkar, K. Ramachandran, U. K. Pal, A. Shrivastava, B. J. Roy, B. K. Nayak, A. Chatterjee, R. K. Choudhury, and S. Kailas, Phys. Lett. B **677**, 139 (2009).

[48] D. Chattopadhyay, S. Santra, A. Pal, A. Kundu, K. Ramachandran, R. Tripathi, D. Sarkar, S. Sodaye, B. K. Nayak, A. Saxena *et al.*, Phys. Rev. C **94**, 061602(R) (2016).

[49] D. Chattopadhyay, S. Santra, A. Pal, A. Kundu, K. Ramachandran, R. Tripathi, B. J. Roy, T. Nag, Y. Sawant, B. K. Nayak *et al.*, Phys. Rev. C **97**, 051601(R) (2018).

[50] C. Beck, N. Keeley, and A. Diaz-Torres, Phys. Rev. C **75**, 054605 (2007).

[51] L. C. Chamon, B. V. Carlson, L. R. Gasques, D. Pereira, C. DeConti, M. A. G. Alvarez, M. S. Hussein, M. A. CandidoRibeiro, E. S. Rossi, and C. P. Silva, Phys. Rev. C **66**, 014610 (2002).

[52] B. Buck *et al.*, J. Phys. G: Nucl. Part. Phys. **14**, L211 (1988).